Hydrodynamics of passing-over motion during binary droplet collision in shear flow*

Cheng-Yao Wang(王程遥)[1], Cheng-Bin Zhang(张程宾)[1], Xiang-Yong Huang(黄庠永)[2], Xiang-Dong Liu(刘向东)[2], and Yong-Ping Chen(陈永平)[1,2,†]

[1] *Key Laboratory of Energy Thermal Conversion and Control of Ministry of Education, School of Energy and Environment, Southeast University, Nanjing* 210096, *China*

[2] *School of Hydraulic, Energy and Power Engineering, Yangzhou University, Yangzhou* 225127, *China*

(Received 14 May 2016; revised manuscript received 2 July 2016; published online 25 August 2016)

A combined experimental and numerical study is undertaken to investigate the hydrodynamic characteristics of single-phase droplet collision in a shear flow. The passing-over motion of interactive droplets is observed, and the underlying hydrodynamic mechanisms are elucidated by the analysis of the motion trajectory, transient droplet deformation and detailed hydrodynamic information (e.g., pressure and flow fields). The results indicate that the hydrodynamic interaction process under shear could be divided into three stages: approaching, colliding, and separating. With the increasing confinement, the interaction time for the passing-over process is shorter and the droplet processes one higher curvature tip and more stretched profile. Furthermore, the lateral separation $\Delta y/R_1$ exhibits larger decrease in the approaching stage and the thickness of the lubrication film is decreased during the interaction. As the initial lateral separation increases, the maximum trajectory shift by the collision interaction is getting smaller. During the collision between two droplets with different sizes, the amplitude of the deformation oscillation of the larger droplet is decreased by reducing the size ratio of the smaller droplet to the bigger one.

Keywords: droplet collision, passing-over motion, hydrodynamics, shear flow

PACS: 82.70.Kj, 83.50.–v, 47.61.Jd, 68.05.–n **DOI:** 10.1088/1674-1056/25/10/108202

1. Introduction

Due to great capacity in versatile manipulation of multi-phase fluids, droplet-based microfluidics has been widely applied in various fields including biological analysis, chemical synthesis, drug delivery systems and materials synthesis.[1–6] Collision between two droplets subjected in an immiscible external flow is a ubiquitous phenomenon involved in the above-mentioned real applications. In particular, the interaction between droplets involves complex free interface hydrodynamics, which is the basic scientific problem in fluidics.[7–10] Additionally, such a complex problem also brings challenges to precisely controlling the interface topology of the droplet in the real application. Therefore, it is of particular interest to fully understand the hydrodynamic mechanisms of colliding droplets subjected to the external flow, so as to realize the active control of single-phase droplet hydrodynamic behaviors.[11,12]

Since the pioneering experimental work by Mason's group,[13–15] several numerical and theoretical studies on the hydrodynamics of droplet collision in the external flow have been carried out.[16–22] However, most of the previous works were concentrated on the detailed behaviors of droplets during their collision.[23–25] It is documented that coalescence between two colliding droplets cannot occur unless the thickness of the liquid film between two droplets is less than a critical one when the van der Waals forces are activated to induce the droplet coalescence.[11,26,27] Generally, without coalescence, two colliding droplets in shear flow experience an irreversible trajectory shift both in the velocity gradient direction and vorticity direction,[18,20] which is defined as passing-over motion. It is worth noting that in the practical application, two closely interacting droplets always undertake the passing-over motion in the concentrated emulsion.[21] Generally, when the initial lateral separation between two droplets is relatively large and the shear flow is less confined, the tendency of passing-over motion is increased for two interacting droplets.[19,20] The detailed droplet behaviors during such motion of two colliding droplets, including droplet shape and moving trajectories, are also found to be determined by the competition among viscous force, surface tension and inertial force involved. For example, large viscous friction offered by a droplet with high viscosity results in strong lubrication force in the thin film, which reduces the tendency of two droplets to come into contact and increases the collision angle before the droplets separate.[22] Large surface tension induces smaller droplet deformation and yields small minimum distances be-

*Project supported by the NSAF (Grants No. U1530260), the National Natural Science Foundation of China (Grant No. 51306158), the Natural Science Foundation of Jiangsu Province, China (Grant No. BK20130621), and the Special Program for Applied Research on Super Computation of the NSFC–Guangdong Joint Fund (the second phase).

†Corresponding author. E-mail: ypchen@seu.edu.cn

© 2016 Chinese Physical Society and IOP Publishing Ltd

tween two interactive droplets during the collision.[28] The big inertia of interactive droplets induces large interaction during the collision, which leads to more compressed droplets and higher trajectory shift in the velocity gradient direction.[19]

In summary, although there are considerable efforts focusing on the hydrodynamics of pairwise single-phase droplet interaction under shear, few experimental data are available about the effects of operation parameters on the interaction behaviors, especially the effects of confinement, initial lateral separation between droplets and size difference between droplets. In addition, the fundamental hydrodynamic mechanisms underlying the droplets interaction and the effects of operation parameters have not been completely known. Therefore, in this work, a visualization experiment and the numerical simulation are combined to elucidate the pairwise collision between single-phase droplets in the shear flow under different operation parameters. In addition, the effects of confinement, initial lateral separation and size difference between droplets on the hydrodynamic interaction of passing-over motion are investigated and analyzed.

2. Experimental and numerical methods

2.1. Experimental method

In the current work, in order to provide the required single-phase droplets for the visualization experiment, we utilized a T-shape micro element[29,30] to produce the single-phase droplets, as shown in Fig. 1(a). The continuous phase, 6-wt% PVA solution (viscosity $\mu_c = 0.132$ Pa·s, density $\rho_c = 1035$ kg·m^{-3}), was prepared by dissolving the PVA particles in distilled water at 60 °C. The dispersed droplet phase, 7-wt% PS organic solution (viscosity $\mu_d = 0.0415$ Pa·s, density $\rho_d = 1051$ kg·m^{-3}) was prepared by dissolving the PS particles in benzene and 1, 2-dichloroethane at 20 °C. All liquids were filtered by the sand-core funnels. The interfacial tension of the PVA–PS interface was measured as $\sigma_{dc} = 0.0226$ N·m^{-1} at 20 °C. In this way, different single-phase droplets were produced through controlling the flow rate of dispersed and continuous phases.

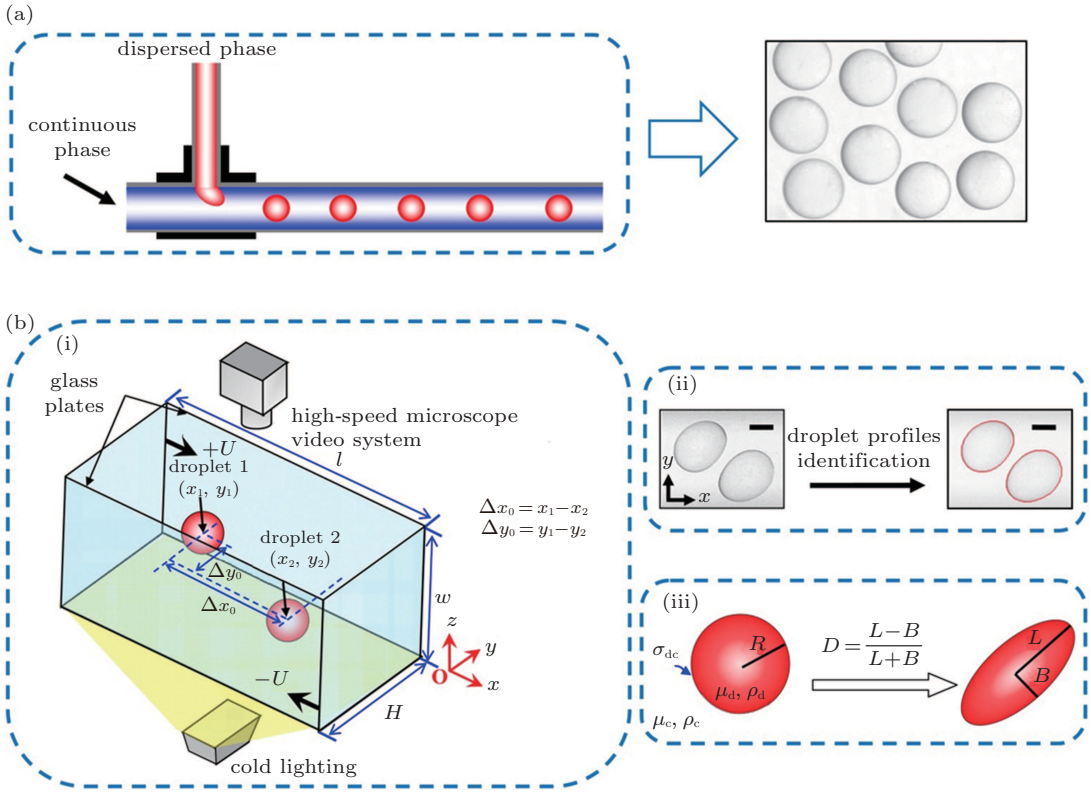


Fig. 1. (color online) (a) Schematic diagram and image of the T-shape microchannel used for generation of the single-phase droplet; (b) (i) Schematic diagram of the experimental setup for observation of droplet collision under shear, (ii) digital solution of experimental image (scale bar = 300 μm), (iii) deformation parameter D.

The experimental apparatus of binary collision of droplets under shear is illustrated in Fig. 1(b). The whole system, placed on a vibration-isolated workstation, consisted of three components: shear flow unit, high-speed microscopy visualization unit and lighting unit. The shear flow system was generated by a typical Couette geometry, where two parallel glass plates were moved reversely with the velocity of U to produce steady shear flow inside with shear rate of $G = 2U/h$. The motion of glass plate was controlled by a motorized precision translation stage (LSDP-300FG). The spacing gap h and parallelism between two plates were both adjusted via a set of tilting, rotary and vertical stages. In the visualization system,

the observation of droplet motion was performed through a stereo microscope (Olympus SZX16) installed with a high-speed video camera (Photron Fastcam SA4), and the droplet motion trajectory was recorded via the computer. In the lighting unit, an LED light source was located below the bottom of the glass tank and a supplementary light source was located above the shear flow apparatus.

Before the experiment, two isolated single-phase droplets were preliminarily injected into the area between two glass plates by a tiny glass capillary and fixed symmetrically around the center of the Couette geometry. As depicted in inset (i) of Fig. 1(b), the initial relative position between centroids of two droplets along the x and y axes can be described as $\Delta x_0/R_1$ ($\Delta x_0 = x_1 - x_2$) and $\Delta y_0/R_1$ ($\Delta y_0 = y_1 - y_2$), respectively. All experiments were performed under ambient temperature of 20 °C.

In order to evaluate the importance of governing forces on the hydrodynamic behaviors of two interactive droplets in shear flow, two important non-dimensional parameters are introduced, which are Reynolds number of the droplet representing the competition of inertia force to viscous shear stress, $Re = \rho_c G R_1^2/\mu_c$, and capillary number of the droplet representing the ratio of viscous shear stress to interfacial tension, $Ca = \mu_c G R_1/\sigma_{dc}$. In the experiment, Re ranges from 0.038 to 0.057, which is far less than 1, implying the current hydrodynamic problem is well within Stokes flow regime.[31] For examining effect of confinement on hydrodynamic behaviors of two interactive droplets, we change the dimensionless confinement, $Co = R_1/h$ (Co = 0.16 ~ 0.2), by adjusting the spacing gap between two plates h and the droplet size R. As depicted in (ii) of Fig. 1(b), a best fit ellipse is obtained by programming to characterize the profiles of deformed interactive droplets, when the sum of squared errors between pixel data of the fitting ellipse and real profile of deformed droplet reaches a minimum. In this way, the deformation degree of the interactive droplets are quantitatively described by the droplet deformation parameters, $D = (L-B)/(L+B)$ by Taylor,[32] where L and B in (iii) of Fig. 1(b) respectively represent the half-length and half-breadth of the best fit ellipse of the droplet. In addition, in order to analyze the effect of size difference on the hydrodynamic behaviors of droplets, we define the size ratio $k = R_2/R_1$ (k = 0.6 ~ 1.0) which is the ratio of the right droplet radius R_2 to the left droplet radius R_1. In the current study, the droplet radius ranges from 288 μm to 493 μm. Note that, herein, the radius of droplet 1 is used as the characteristic scale to define the hydrodynamic and geometric parameters. In addition, since two droplets with approximately identical size deform with nearly the same degree during the collision, the deformation parameter of droplet 1 is chosen as D to represent the deformation degree of two droplets.

2.2. Numerical method

In order to gain a deeper understanding of the hydrodynamics underlying the droplet interaction under shear, a numerical simulation is also performed to elucidate the specified hydrodynamic information between two interactive droplets which involves the interface structure, pressure distribution and the flow field structure. The volume of fluid (VOF) method[33] is adopted to track the free interfaces during the droplet interaction. In the VOF method, the continuous phase and the dispersed phase are regarded as incompressible fluids, and the volume fraction of the phase fluid is defined as α. In each computational cell, α lies between 0 and 1, where

$$\alpha = \begin{cases} 1, & \text{continuous phase fluid only,} \\ 0 < \alpha < 1, & \text{liquid–liquid interface,} \\ 0, & \text{dispersed phase fluid only.} \end{cases} \tag{1}$$

The volume fraction α is governed by a transport equation

$$\frac{\partial \alpha}{\partial t} + \boldsymbol{u} \cdot \nabla \alpha = 0, \tag{2}$$

where t is time and $\boldsymbol{u}$ is the velocity of the fluid.

Depending on the values of volume fraction, the Navier–Stokes equations for incompressible fluids are solved in the computational domain as:

$$\nabla \cdot \boldsymbol{u} = 0, \tag{3}$$

$$\rho\left(\frac{\partial \boldsymbol{u}}{\partial t} + \boldsymbol{u} \cdot \nabla \boldsymbol{u}\right) = -\nabla p + \nabla \cdot \left[\mu\left(\nabla \boldsymbol{u} + \nabla \boldsymbol{u}^T\right)\right] + \boldsymbol{F}_s, \tag{4}$$

where p is the pressure, and the fluid properties ρ and μ are the density and the viscosity which are updated by the volume fraction of each cell,

$$\rho = \alpha\rho_c + (1-\alpha)\rho_d, \tag{5}$$

$$\mu = \alpha\mu_c + (1-\alpha)\mu_d. \tag{6}$$

The term $\boldsymbol{F}_s$ represents the surface tension force by the continuum surface force (CSF) model,

$$\boldsymbol{F}_s = \sigma \frac{\rho\kappa\nabla\alpha}{(1/2)(\rho_c + \rho_d)}, \tag{7}$$

where σ is the interfacial tension coefficient and κ is the mean curvature of the free surface, which is defined in the terms of the divergence of the unit normal $\boldsymbol{n}_s$:

$$\kappa = \nabla \cdot \boldsymbol{n}_s, \quad n_s = \frac{\nabla\alpha}{|\nabla\alpha|}. \tag{8}$$

In the simulation, the governing equation mentioned before are numerically solved by the control volume finite-difference technique. The semi-implicit method for pressure linked equation (SIMPLE) algorithm is utilized for pressure–velocity coupling, and first-order upwind differencing scheme is adopted to discretize momentum equation. The piecewise linear interface calculation (PLIC) algorithm is employed

for the liquid–liquid interface reconstruction. The under-relaxation factors are used at values: 0.2 (pressure), 0.5 (density), 0.5 (body force), 0.2 (momentum), with which the numerical calculation possesses good convergence and high efficiency. The no-slip boundary conditions are applied to the walls of two parallel moving plates and periodical boundary conditions are applied to the remaining boundaries. Due to the surface tension, there is a Laplace jump across every interface. We adopted the dynamically adaptive mesh refinement[34] to solve the computations on the important regions with high pressure and velocity gradient and the area of interfaces. In consideration of the simulation with diverse grid and time step resolutions, good convergences in space and in time have also been verified to warrant the reliable numerical results.

A comparison between the two-dimensional (2D) and three-dimensional (3D) numerical simulations of binary droplet interaction under shear flow have been performed in Fig. 2. As shown in Fig. 2, the 2D numerical results of droplet shape evolution and the relative trajectory during the interaction are similar to the 3D results within the acceptable error. Accordingly, taking both considerations of computational efficiency and reasonability, the 2D numerical simulation is adopted in the current study.

Herein, a spatial and temporal convergence study is conducted to under various mesh sizes ($\Delta x = \Delta y = R_1/8$, $R_1/12$, $R_1/16$, $R_1/20$) and various dimensionless time step sizes ($\Delta t = 5.0 \times 10^{-4}$, 2.5×10^{-3}, 5×10^{-3}, 2.5×10^{-2}) with the definition of $\Delta t = t_s G$, where t_s is the realistic time step, which is depicted in Fig. 3. It can be seen that the results converge with the refinement of mesh and there is little difference in simulation results between the mesh sizes of $R_1/16$ and $R_1/20$ in Fig. 3(a). In addition, as shown in Fig. 3(b), the droplet deformation results are insensitive to the numerical time step size which is less than 2.5×10^{-3}. In consideration with the reasonable computational time and the accuracy of numerical results, the mesh size $\Delta x = \Delta y = R_1/16$ and time step size $\Delta t = 2.5 \times 10^{-3}$ are utilized in this study.

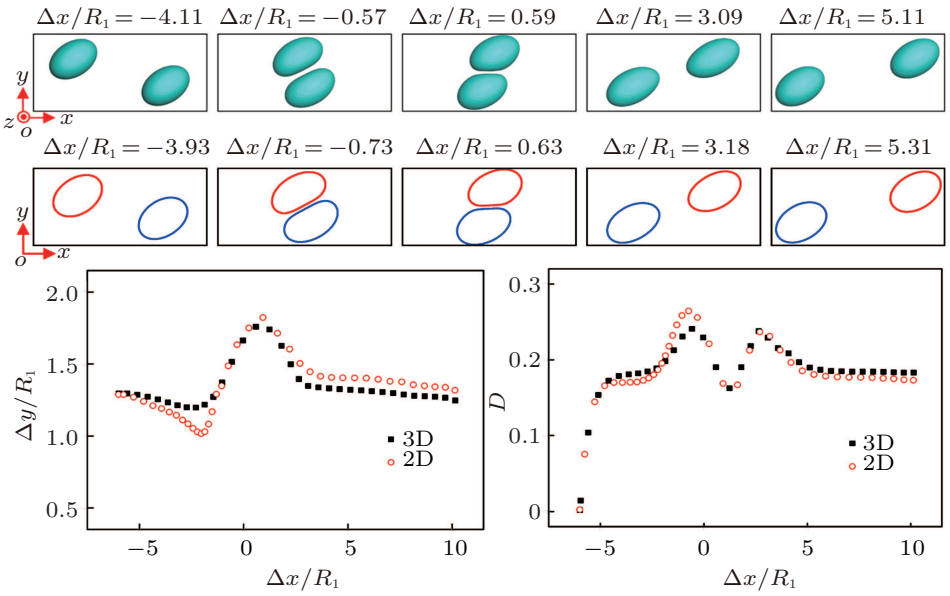


Fig. 2. (color online) Comparison of the results in two- and three-dimensional domain.

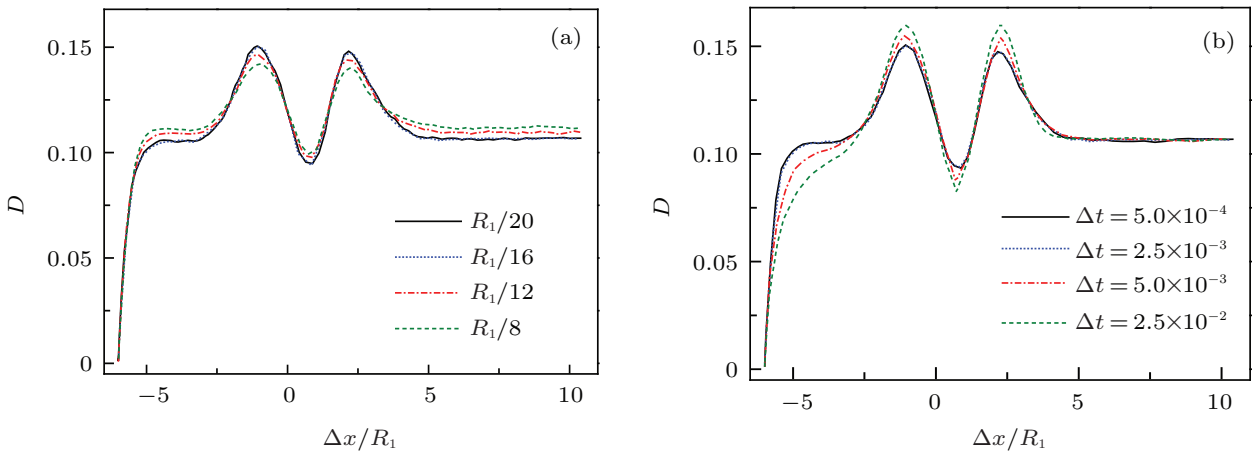


Fig. 3. (color online) Simulation results for spatial and temporal convergence study: (a) droplet deformation under four different meshes; (b) droplet deformation under four different time step sizes.

3. Results and discussion

3.1. Typical single-phase droplet collision hydrodynamics

Within the current experimental conditions, the typical passing-over motion of interactive droplets is observed, when the droplets pass over each other during the droplet interaction under shear, as shown in Fig. 4(a). In order to obtain a deep insight into this typical collision motion, a numerical simulation is performed to provide the specified hydrodynamic information behind the passing-over motion, including temporal evolution of pressure and velocity distributions, as depicted in Fig. 5. The good agreement between experimental and numerical results on hydrodynamic behaviors of passing-over motion verifies the reasonability of current theoretical model. Note that it is indicated that the hydrodynamic interaction process under shear could be divided into three stages: approaching, colliding and separating.

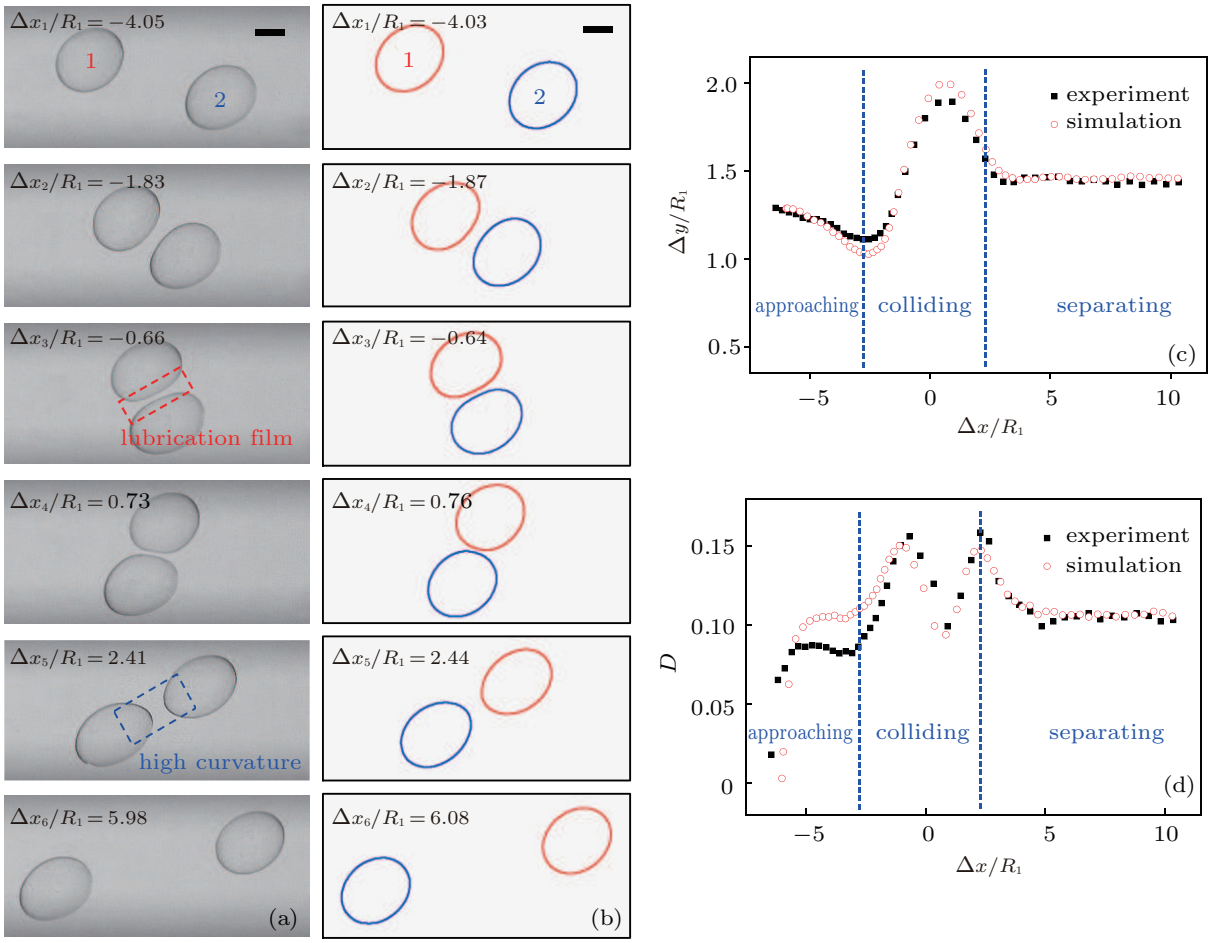


Fig. 4. (color online) Motion behaviors of single-phase droplet collision under shear (Co = 0.16, Ca = 0.10, k =1) in experiment and simulation: (a) droplet shape evolution in experiment (scale bar = 300 μm); (b) droplet shape evolution in simulation (scale bar = 300 μm); (c) relative trajectory; (d) droplet deformation.

At the approaching stage, induced by the applied shear flow, the droplets experience fast deformation to be ellipsoidal [$\Delta x_1/R_1 = -4.05$ in Fig. 4(a)]. As two single-phase droplets approach each other, the lateral separation between two droplets $\Delta y/R_1$ gradually decreases to a minimum value, as shown in the Fig. 4(c), by the local entrainment of the streams developed in the continuous phase which is marked by a dashed box in $\Delta x_1/R_1 = -4.05$ in Fig. 5(b).

During the colliding stage, the lateral separation $\Delta y/R_1$ sharply increases to reach a maximum value (Fig. 4(c)). When the droplet comes into contacting with the other droplet, two droplets squeeze each other and drain the continuous liquid between them, with a high-pressure region and liquid lubrication film formed between two droplets [$\Delta x_2/R_1 = -1.87$ in Fig. 5(a)]. As the liquid lubrication film is thinning, the high-pressure region there continues pressing the droplet interface, and then produces a flat contact area until the deformation of droplet reaches the first maximum value [$\Delta x_3/R_1 = -0.64$ in Fig. 5(a)]. Subsequently, two droplets climb over each other to the top. At this time, the maximum lateral separation $\Delta y/R_1$ occurs [$\Delta x_4/R_1 = 0.73$ in Fig. 4(a)], and interaction between two droplets is receding, which causes the relaxation of deformed droplet with the droplet getting the minimum deformation.

When the interaction comes into the separating stage, droplets separate and recoil with a high curvature tip until

they get the second maximum deformation [$\Delta x_5/R_1$ = 2.41 in Fig. 4(a)], which is induced by suck effect on the interface of the droplet tip. The suck effect can be explained by the simulation results from $\Delta x_5/R_1$ = 2.44 in Fig. 5(a) that there is a low-pressure region formed between two droplets (as marked in $\Delta x_5/R_1$ = 2.44 in Fig. 5(a)), where a large pressure gradient is developed across the droplet interface that generates 'suck', resulting in a high curvature there. In the later separating stage, two droplets fully separate with steady ellipsoidal shape and the lateral separation between them $\Delta y/R_1$ gets a new larger value due to the interaction at contacting stage, making the droplets move into new shear streams closer to the walls [$\Delta x_6/R_1$ = 5.98 in Fig. 4(a)].

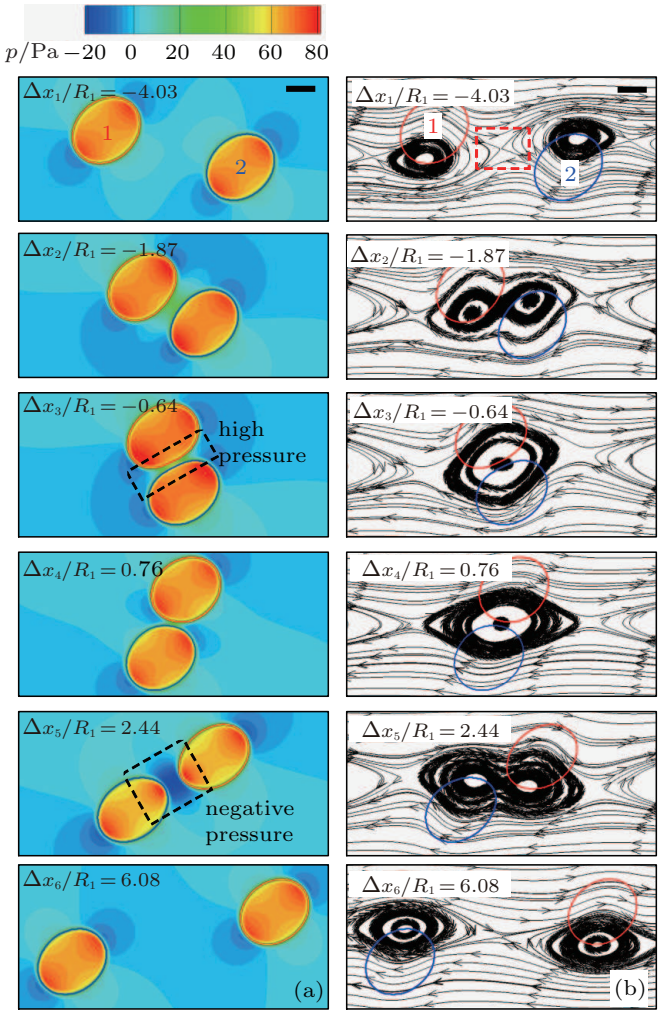


Fig. 5. (color online) Local transient pressure and velocity contour for passing-over motion (Co = 0.16, Ca = 0.10, k =1): (a) pressure contour (scale bar = 300 μm); (b) velocity contour (scale bar = 300 μm).

3.2. Effects of operation parameters on the collision hydrodynamics

3.2.1. Confinement

Compared with unbounded shear flow, the confined shear flow involves more obvious wall effect, which affects the characteristics of flow field in continuous flow and thus induces different hydrodynamics of the droplet subjected into it.[35] Figure 6 depicts the effect of confinement on droplet hydrodynamic behaviors under shear flow. Herein, we introduce "collision time" to evaluate the duration of collision, which is calculated from $\Delta x/R_1 = -4$ to $\Delta x/R_1 = 6$. As shown in Figs. 6(a) and 6(b), the "collision time" at confinement of 0.20 is 2.37 s, which is shorter than 3.09 s at confinement of 0.16. This can be explained by the additional drag force caused by the wall effect under a confined shear flow, and it can be demonstrated by the hydrodynamic information illustrated in Fig. 7. As indicated in Fig. 7(a), owing to the wall effect, the extreme value of the shear rate and the elongational components at the droplet tip near the wall are higher under more confined shear flow [(iii) in Fig. 7(a)]. This produces an additional drag force on the droplets with respect to the unconfined shear flow, which increases the droplet velocity during the hydrodynamic interaction and thus shortens the whole collision process. In addition, due to the additional drag force and the larger viscous shear force caused by the wall effect at the confinement of 0.20, the droplet exhibits more stretched asymmetric spheroidicity shape with a high curvature tip close to the wall during the whole collision process. As shown in the Fig. 7(b), a larger pressure gradient also occurs across the interface at this high curvature tip with respect to that at the other obtuse tip. Furthermore, as shown in the Fig. 6(c), the lateral separation $\Delta y/R_1$ exhibits larger decrease in the approaching stage under more confined shear flow, implying bigger reaction of the wall imposed on the droplet perpendicularly to the shear during the collision. This perpendicular reaction by the wall also makes two droplets get closer to each other, and thus decreases the thickness of the lubrication film during interaction [as marked by dashed box in Fig. 6(a) and 6(b)].

3.2.2. Initial lateral separation

The initial lateral separation also plays an important role in the hydrodynamic behaviors of two interactive droplets under shear flow. Figure 8 illustrates the effects of initial lateral separation on the transient droplet deformation and the relative trajectory of the droplets under shear. Actually, the increase in initial separation $\Delta y_0/R_1$ under the same Co implies that the droplet is closer to the wall region with large drag force. Moreover, the big initial separation $\Delta y_0/R_1$ produces small collision strength and short interaction time. Therefore, the time for the collision process at $\Delta y_0/R_1$ of 1.57 is shorter than 1.82 s at $\Delta y_0/R_1$ of 1.23, as shown in Figs. 8(a) and 8(b). Moreover, due to the small collision interaction strength and time at large $\Delta y_0/R_1$, the maximum trajectory shift by the collision interaction is small under $\Delta y_0/R_1$ = 1.57, as depicted in Fig. 8(c), and less liquid is squeezed out of the lubrication film between two interacting droplets, resulting in thicker lubrication film, as compared in Fig. 9.

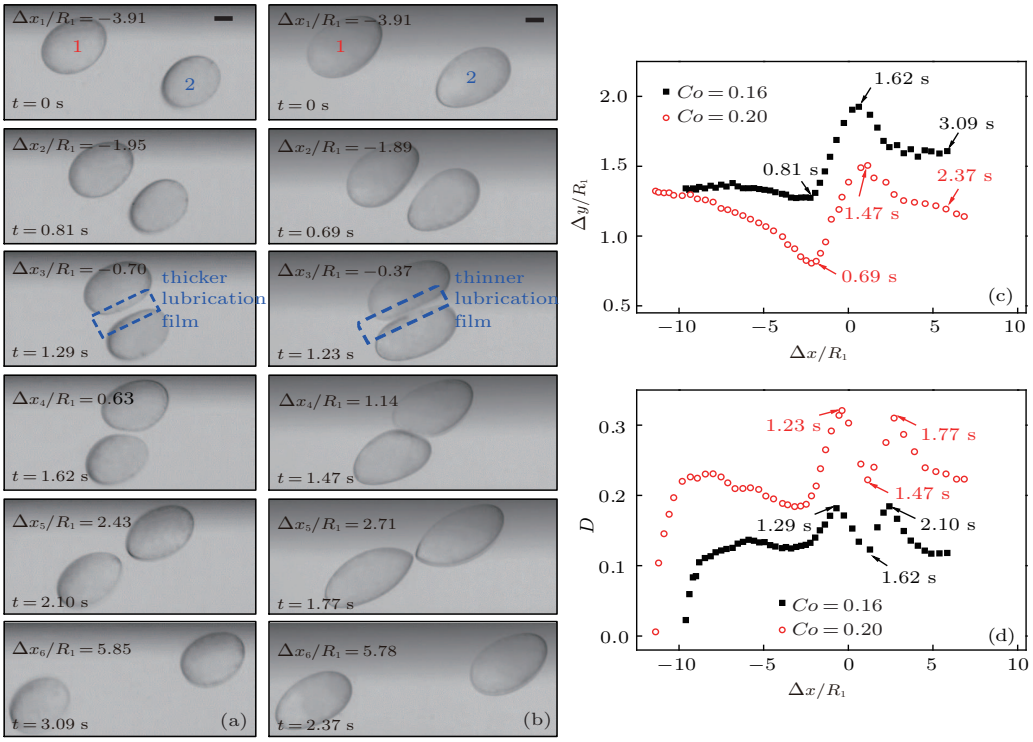


Fig. 6. (color online) Effect of confinement on droplet rheological behaviors (Ca = 0.10): (a) motion behaviors (Co = 0.16, k =1, scale bar = 300 μm); (b) motion behaviors (Co = 0.20, k =1, scale bar = 300 μm); (c) relative trajectory; (d) droplet deformation.

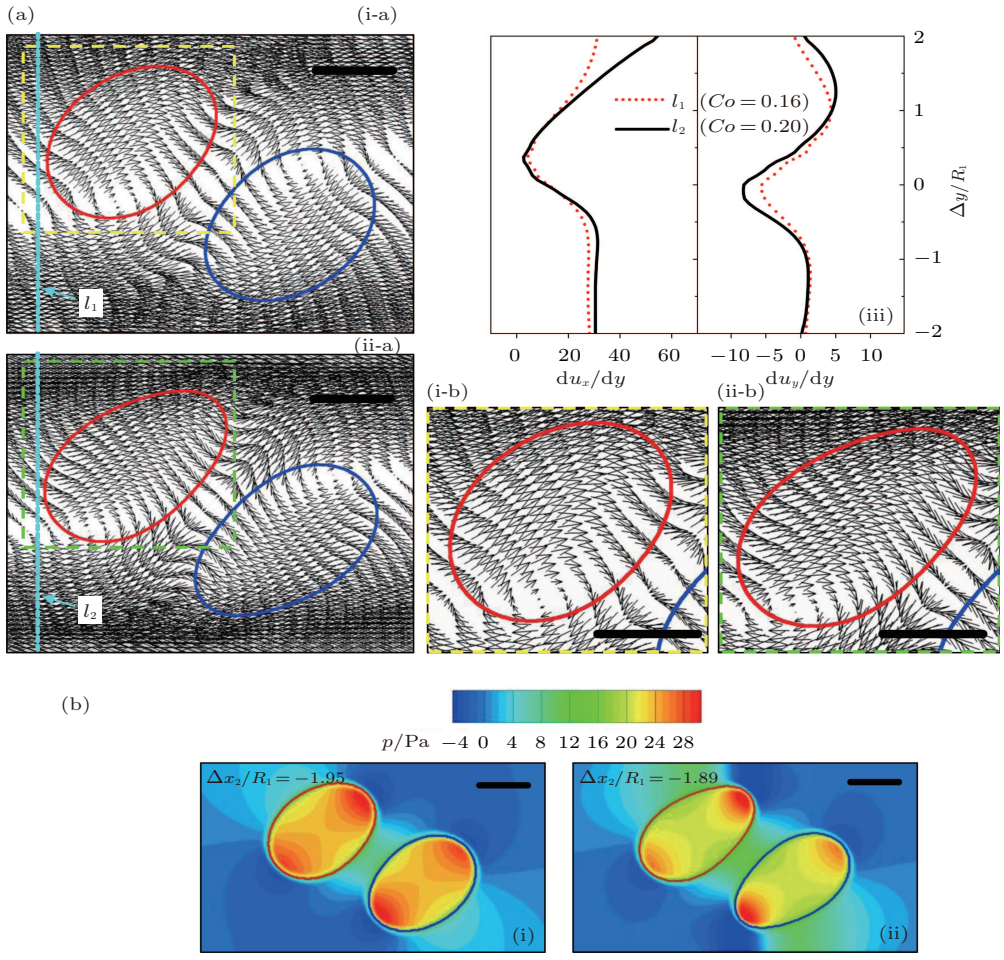


Fig. 7. (color online) Effect of confinement on droplet rheological behaviors (Ca = 0.10, k =1): (a) (i-a, i-b) local flow field (Co = 0.16, scale bar = 300 μm), (ii-a, ii-b) local flow field (Co = 0.20, scale bar = 300 μm), (iii) elongational component du_y/dy and shear rate du_x/dy for x fixed at the value where the highest elongational component of the velocity field are attained; (b) (i) local pressure field (Co = 0.16, scale bar = 300 μm), (ii) local pressure field (Co = 0.20, scale bar = 300 μm).

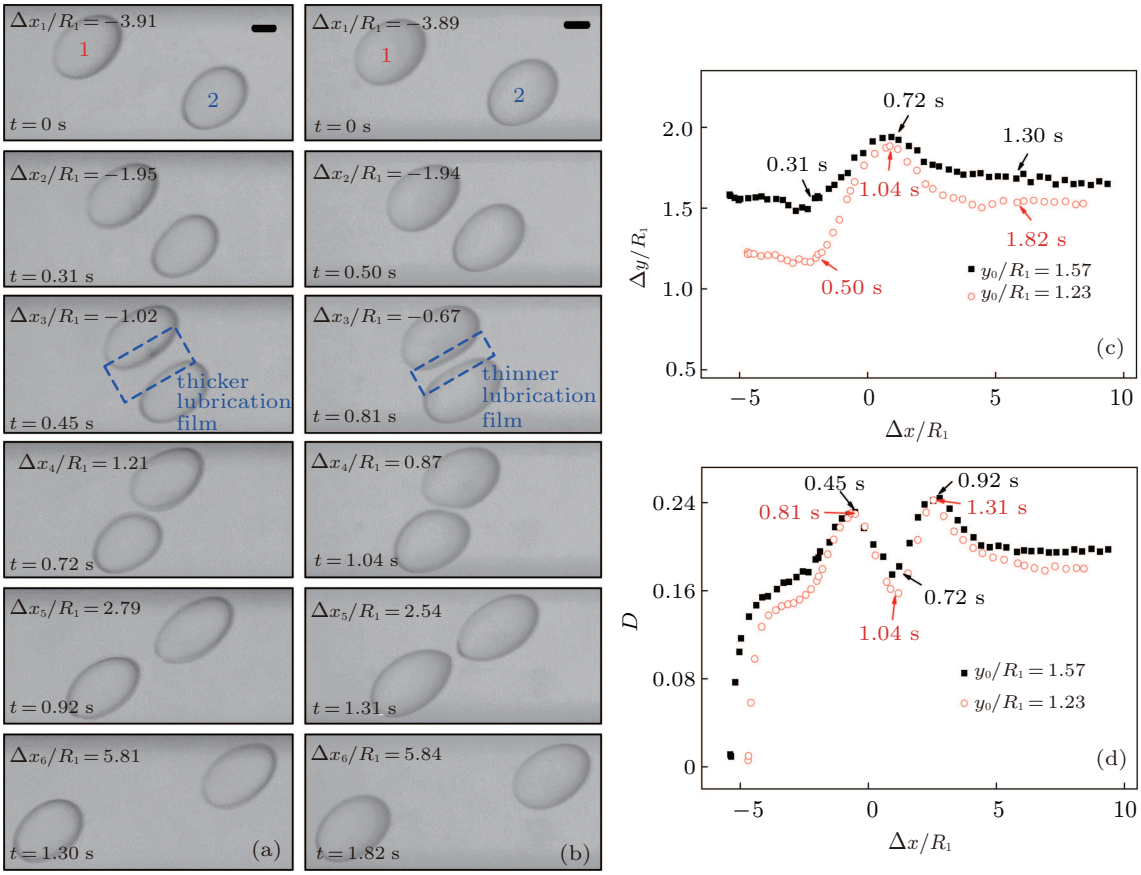


Fig. 8. (color online) Effect of initial lateral separation on droplet rheological behaviors (Co = 0.15, Ca = 0.14): (a) motion behaviors (y_0/R_1 = 1.57, k =1, scale bar = 300 μm); (b) motion behaviors (y_0/R_1 = 1.23, k =1, scale bar = 300 μm); (c) relative trajectory; (d) droplet deformation.

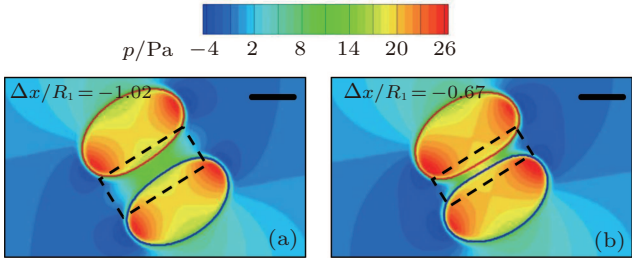


Fig. 9. (color online) Effect of initial lateral separation on droplet rheological behaviors (Co = 0.15, Ca = 0.14, k = 1, scale bar = 300 μm): (a) local pressure field (y_0/R_1 = 1.57); (b) local pressure field (y_0/R_1 = 1.23).

3.2.3. Size difference between two droplets

Figures 10 and 11 illustrate the effect of size difference between two interacting droplets on the collision hydrodynamics. Herein, the size ratio $k = R_2/R_1$ is defined to characterize the size difference between two interacting droplets, where R_2 is the radius of the lower droplet and R_1 is that of the upper one. It can be seen from Fig. 10 that (k = 0.77), compared with the small droplet, the large droplet has a large droplet deformation. This is mainly attributed to the fact that the small droplet with large interface curve possesses the big interface tension to hold itself in a spherical shape. The numerical results in Fig. 11 also demonstrate this reason that the large pressure occurs in the small droplet induced by the large interfacial tension due to the small curve radius of interface. Moreover, figure 11 compares the numerical hydrodynamics of droplets collision under

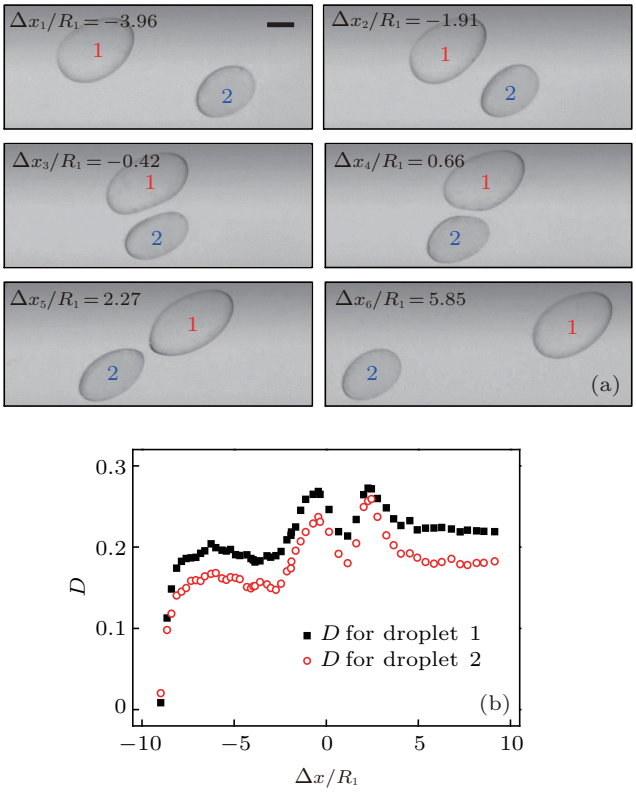


Fig. 10. (color online) Effect of size difference on droplet rheological behaviors (Co = 0.13, Ca = 0.12, k = 0.77): (a) motion behaviors (scale bar = 300 μm); (b) droplet deformation.

various size ratios. As depicted in inset (i) of Fig. 11(a), with the decrease in k, the maximum $\Delta y/R_1$ in the colliding stage is smaller. In addition, the amplitude of the deformation oscillation of droplet 1 is decreased by the reduction of k, as depicted in inset (ii) of Fig. 11(a). These are mainly because the initial inertia of the droplet 2 before collision is reduced by the decrease in its size (i.e. droplet in k), leading to less interaction of droplet 2 with droplet 1 during the collision. In addition, the smaller droplet with larger interface tension is stronger to resist the deformation. Therefore, droplet 2 exhibits smaller deformation and deformation oscillation with its decreasing size (i.e. reducing k), as indicated in inset (iii) of Fig. 11(a).

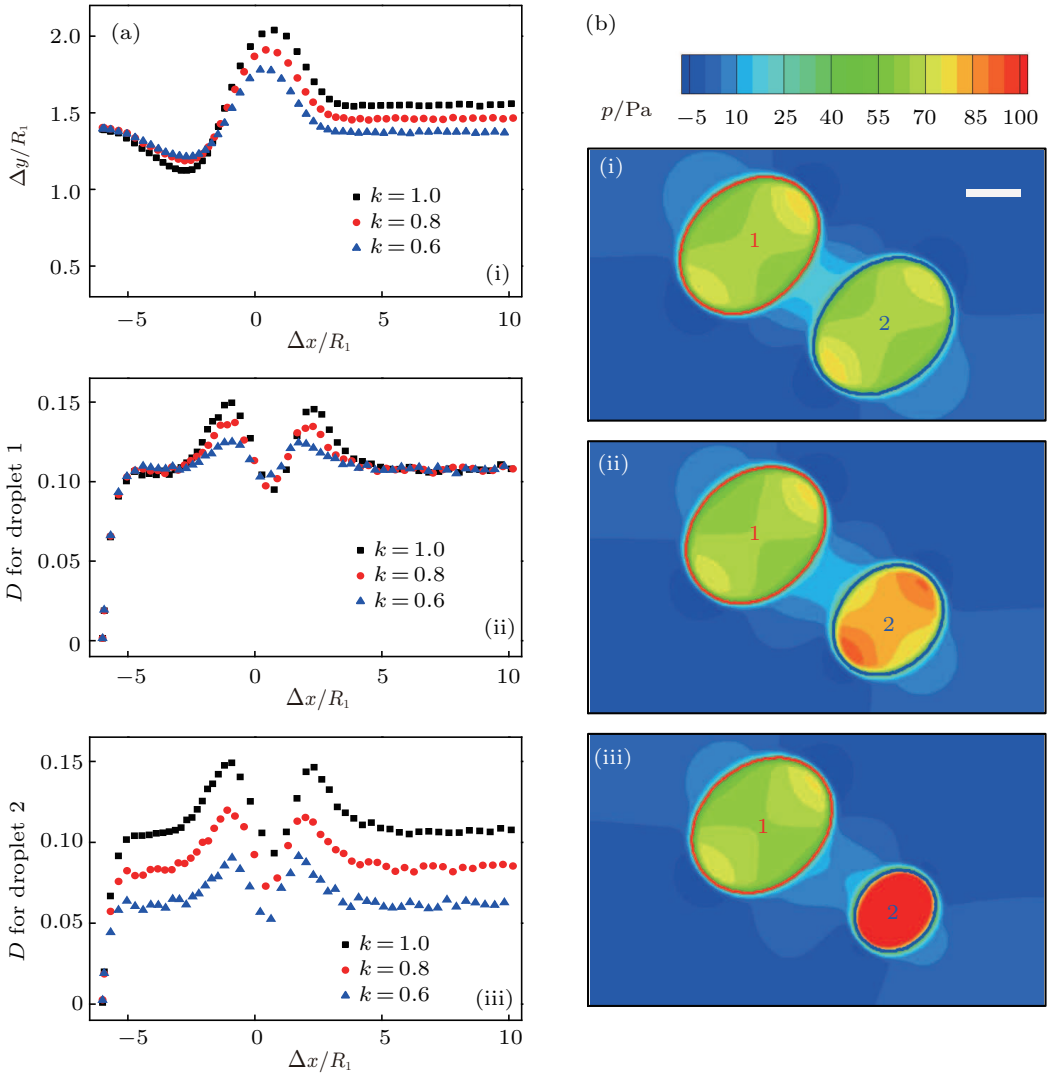


Fig. 11. (color online) Effect of size difference on droplet rheological behaviors (Co = 0.16, Ca = 0.10, k = 0.6 ∼ 1): (a) (i) deformation for droplet 1, (ii) deformation for droplet 2; (b) (i) local pressure field (k = 1, scale bar = 300 μm), (ii) local pressure field (k = 0.8), (iii) local pressure field (k = 0.6).

4. Conclusions

In this article, via combining the experimental observation with numerical simulation, the hydrodynamic characteristics of single-phase droplet collision in a shear flow are explored. The passing-over motion of interactive droplets is observed, and the hydrodynamic behaviors of the droplets are quantitatively characterized by the motion trajectory, transient droplet deformation and local pressure contour. The effects of the confinement, initial lateral separation and size difference between two droplets are examined and analyzed. The hydrodynamic interaction of the passing-over process under shear could be divided into three stages: approach, collision and separation. At the approaching stage, $\Delta y/R_1$ gradually decreases to a minimum value by the local entrainment of the streams and the droplets are stretched to be ellipsoidal. At the colliding stage, $\Delta y/R_1$ sharply increases to reach a maximum value and droplets undergo the first maximum deformation and the minimum deformation. At the separation stage, $\Delta y/R_1$ gets a new larger value due to the interaction and the droplets undergo the second maximum deformation then reach a new steady deformation. With the increasing confinement, the wall effect of the shear flow on the droplet is enhanced and that induces the additional drag force and larger viscous shear force, which makes the interaction time for the passing-over process shorter and the droplets process one higher curvature

tip and more stretched profile. Furthermore, the lateral separation $\Delta y/R_1$ exhibits larger decrease in the approaching stage and the thickness of the lubrication film is decreased during the action. As the initial lateral separation increases, the interaction time is shorter during the interaction, and the collision strength is smaller which makes less liquid between two droplets squeeze out, resulting in thicker lubrication film. In addition, with the larger lateral separation, the maximum trajectory shift by the collision interaction is small. During the collision between two droplets with different sizes, the amplitude of the deformation oscillation of the larger droplet is decreased by reduction of the size ratio of smaller droplet to the bigger one. In addition, as a result of the small droplet possessing larger interface tension to resist the deformation, the smaller droplet exhibits smaller deformation and deformation oscillation.

References

[1] Wang J T, Wang J and Han J J 2011 *Small* **7** 1728
[2] DeMello A J 2006 *Nature* **442** 394
[3] Hu H B, Huang S H and Chen L B 2013 *Chin. Phys. B* **22** 084702
[4] Zhao Y J, Shum H C, Chen H S, Adams L L A, Gu Z Z and Weitz D A 2011 *J. Am. Chem. Soc.* **133** 8790
[5] Dittrich P S and Manz A 2006 *Nat. Rev. Drug Discov.* **5** 210
[6] Zhao Y J, Gu H C, Xie Z Y, Shum H C, Wang B P and Gu Z Z 2013 *J. Am. Chem. Soc.* **135** 54
[7] Lee M W, Kang D K, Yoon S S and Yarin A L 2012 *Langmuir* **28** 3791
[8] Zhang L and She W L 2015 *Chin. Phys. B* **24** 104207
[9] Wang H, Liao Q, Zhu X, Li J and Tian X 2010 *J. Supercond. Nov. Magn.* **23** 1165
[10] Tian F B, Wang W Q, Wu J and Sui Y 2016 *Comput. Fluids* **124** 1
[11] Liu Z, Chan S T, Faizi H A, Roberts R C and Shum H C 2015 *Lab Chip* **15** 2018
[12] Chen X D, Song Y X, Li D Q and Hu G Q 2015 *Phys. Rev. Appl.* **4** 024005
[13] Bartok W and Mason S G 1959 *J. Colloid Sci.* **14** 13
[14] Allan R S and Mason S G 1962 *J. Colloid Sci.* **17** 383
[15] Mackay G D and Mason S G 1964 *Kolloid-Z.* **195** 138
[16] Loewenberg M and Hinch E J 1996 *J. Fluid Mech.* **321** 395
[17] Loewenberg M and Hinch E J 1997 *J. Fluid Mech.* **338** 299
[18] Lac E and Barthès-Biesel D 2008 *Phys. Fluids* **20** 040801
[19] Olapade P O, Singh R K and Sarkar K 2009 *Phys. Fluids* **21** 063302
[20] Singh R K and Sarkar K 2009 *Phys. Fluids* **21** 103303
[21] Bayareh M and Mortazavi S 2011 *Int. J. Multiph. Flow* **37** 1315
[22] Bayareh M and Mortazavi S 2011 *Adv. Eng. Softw.* **42** 604
[23] Guido S and Simeone M 1998 *J. Fluid Mech.* **357** 1
[24] Chen D J, Cardinaels R and Moldenaers P 2009 *Langmuir* **25** 12885
[25] Bruyn P D, Chen D J, Moldenaers P and Cardinaels R 2014 *J. Rheol.* **58** 1955
[26] Klaseboer E, Chevaillier J Ph, Gourdon C and Masbernat O 2000 *J. Colloid Interface Sci.* **229** 274
[27] Shardt O, Mitra S K and Derksen J J 2014 *Langmuir* **30** 14416
[28] Xu J J, Li Z L, Lowengrub J and Zhao H K 2011 *Commun. Comput. Phys.* **10** 453
[29] Garstecki P, Fuerstman M J, Stone H A and Whitesides G M 2006 *Lab Chip* **6** 437
[30] Xu J H, Li S W, Tan J, Wang Y J and Luo G S 2006 *AIChE J.* **52** 3005
[31] Renardy Y Y and Cristini V 2001 *Phys. Fluids* **13** 2161
[32] Taylor G I 1934 *Proc. R. Soc. A* **146** 501
[33] Hirt C W and Nichols B D 1981 *J. Comput. Phys.* **39** 201
[34] Chen X D and Yang V 2014 *J. Comput. Phys.* **269** 22
[35] Sibillo V, Pasquariello G, Simeone M, Cristini V and Guido S 2006 *Phys. Rev. Lett.* **97** 054502